Electronic Supplementary Information

The effect of dopants chirality on the properties of the chiral smectic C phase

Dorota Węgłowska*, Paweł Perkowski, Maciej Chrunik and Michał Czerwiński

Faculty of Advanced Technologies and Chemistry, Military University of Technology,
2 Kaliskiego Str., 00-908 Warsaw 49, Poland
*Email: dorota.weglowska@wat.edu.pl

1 Preparative procedures

The purity of intermediates and the main compounds were determined by thin layer chromatography (TLC), GC-MS(EI) (Agilent 6890N, Santa Clara, CA, USA) and HPLC-PDAMS(API-ESI) (Shimadzu Prominence LC20) chromatography systems. The structures of the final compounds were confirmed by mass spectra registered on HPLC chromatography system with a diode array detector (SPD-M20A) and mass detector (LCMS-85 2010EV) and by ^{1}H and ^{1}C NMR spectroscopy (Bruker, Avance III HD, 500 Hz; $CDCl_3$, Billerica, MA, USA).

Synthetic details are described for an exemplary compound 3FO2C5.

1.6 4'-[2-(2,2,3,3,4,4,4-heptafluorobutoxy)etoxy]biphenyl-4-yl 3-pentyloxybenzoate (3FO2C5)

A mixture of (*S*)-(+)-4'-hydroxybiphenyl-4-yl 4-(octan-2-yloxy)benzoate (**8b**) (1.0 g; 0.0027 mol), 2-(2,2,3,3,4,4,4-heptafluorobutoxy) ethanol (0.84 g; 0.0035 mol), triphenylphosphine (0.91 g; 0.0035 mol), diisopropyl azodicarboxylate (0.70 g; 0.0035 mol) and dry THF (30 ml) was stirred at room temperature until the reaction was completed (TLC). Then the solvent was evaporated to dryness and the residue was purified on chromatography column (SiO_2/CH_2Cl_2). The product was crystallized from ethanol twice (2×40 ml). A white solid was obtained. Yield: 0.82 g (50.9%); purity (HPLC): 99.0%; MS: 602 $[M+H]^+$, 639 $[M+Na]^+$.

In similar way were obtained:

1.7 4'-[3-(2,2,3,3,4,4,4-heptafluorobutoxy)propoxy]biphenyl-4-yl 3-pentyloxybenzoate (3FO3C5)

Yield: 0.79 g (79.7%); purity (HPLC) 99.8%; MS: 616 $[M+H]^+$, 653 $[M+Na]^+$.

1.7 4'-[3-(2,2,3,3,4,4,4-heptafluorobutoxy)butoxy]biphenyl-4-yl 3-pentyloxybenzoate (3FO4C5)

Yield: 0.82 g (61.0%); purity (HPLC)>99.9%; MS: 630 $[M+H]^+$, 652 $[M+Na]^+$.

1.8 4'-[5-(2,2,3,3,4,4,4-heptafluorobutoxy)pentyloxy]biphenyl-4-yl 3-pentyloxybenzoate (3FO5C5)

Yield: 0.48 g (41.7%); purity (HPLC): >99.9%; MS: 644 $[M+H]^+$, 666 $[M+Na]^+$;

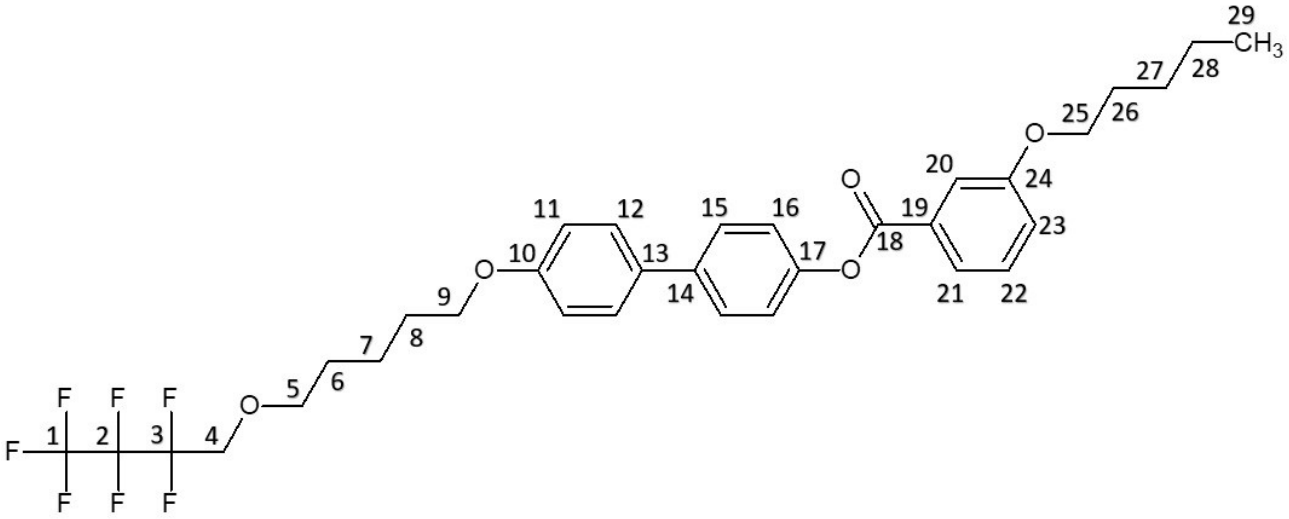

^{1}H NMR ($CDCl_3$) δ/ppm: 0.97 (*t*, 3H, -CH_3, **29**), 1.00 (*t*, 3H, -CH_3; **26**), 1.39-1.89 (*m*, 12H, -CH_2-; **28**, **27**, **26**, **6**, **7**, **8**), 3.67 (*t*, 2H, -CH_2-; **5**), 3.95 (*t*, 4H, -CH_2-; **9**, **25**), 4.06 (*m*, 2H, -CH_2-; **4**), 6.98 (*d*, 2H, Ar-H; **16**), 7.19 (*d*, 1H, Ar-H; **21**), 7.27 (*d*, 1H, Ar-H; **23**), 7.44 (*t*, 1H, Ar-H; **22**), 7.53 (*d*, 2H, Ar-H; **12**), 7.62 (*d*, 1H, Ar-H; **20**), 7.74 (*d*, 1H, Ar-H; **16**), 7.83 (*d*, 1H, Ar-H; **21**);

^{1}C NMR ($CDCl_3$) δ/ppm: 14.0 (**29**), 22.4 (**28**), 22.5 (**7**), 28.2 (**27**), 25.0 (**6**), 28.9 (**26**), 29.0 (**8**), 29.2 (**4**), 67.4 (**9**), 67.6 (**5**), 67.8 (**25**), 67.6 (**2**), 68.3 (**20**), 73.0 (**1**), 114.8 (**11**), 115.3 (**3**), 120.6 (**23**), 121.9 (**21**), 122.4 (**16**), 127.7 (**22**), 128.1 (**12**), 129.6 (**15**), 130.8 (**13**), 132.9 (**19**), 138.7 (**14**), 149.9 (**17**), 158.7 (**24**), 159.3 (**10**), 165.2 (**18**).

1.9 4'-[7-(2,2,3,3,4,4,4-heptafluorobutoxy)heptyloxy]biphenyl-4-yl 3-pentyloxybenzoate (3FO6C5)

Yield: 0.46 g (38.7%); purity (HPLC): 99.8%; MS: 658 $[M+H]^+$, 688 $[M+Na]^+$.

1.11 4'-[2-(2,2,3,3,4,4,4-heptafluorobutoxy)etoxy]biphenyl-4-yl 4-(octan-2-yloxy)benzoate (C1C1)

A mixture of (*S*)-(+)-4'-hydroxybiphenyl-4-yl 4-(octan-2-yloxy)benzoate (**8b**) (0.75 g, 0.0018 mol), (*R*)-2-octanol (0.30 g, 0.0023 mol), triphenylphosphine (0.51g, 0.0023 mol), diisopropyl azodicarboxylate (0.46 g, 0.0023 mol) and dry THF (30 ml) was stirred at room temperature until the reaction was completed (TLC). Then the solvent was concentrated to the dryness, and the residue was purified on chromatography column (SiO_2/CH_2Cl_2) and crystallised from ethanol twice (2×50 ml). A white solid was obtained. Yield: 0.92 g (66.4%); purity (HPLC): 99.6%; MS: 530 $[M+H]^+$, 552 $[M+Na]^+$;

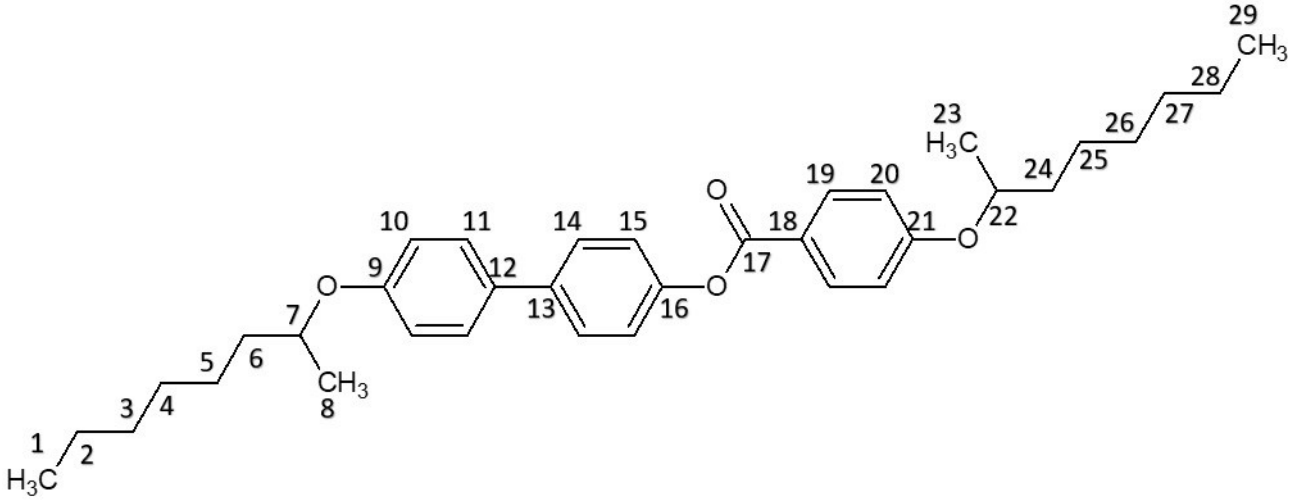

^{1}H NMR ($CDCl_3$) δ/ppm: 0.91 (*t*, 6H, -CH_3, **29**, **1**), 1.33-1.83 (*m*, 16H, -CH_2-; **26**, **4**, **2**, **3**, **28**, **27**, **6**, **24**), 1.38 (*d*, 6H, **8**, **23**), 4.42 (*m*, 1H, -CH_2-, **22**), 4.50 (*m*, 1H, -CH_2-, **7**), 6.98 (*s*, 2H, Ar-H; **10**), 6.99 (*s*, 2H, Ar-H; **15**), 7.28 (*d*, 2H, Ar-H; **20**), 7.52 (*d*, 2H, Ar-H; **11**), 7.60 (*d*, 2H, Ar-H; **14**), 8.18 (*d*, 2H, Ar-H; **19**).

^{1}C NMR ($CDCl_3$) δ/ppm: 14.0 (**1**), 22.4 (**29**), 22.5 (**8**), 28.2 (**23**), 25.0 (**2**), 28.9 (**28**), 29.0 (**5**), 29.2 (**25**), 67.4 (**4**), 67.6 (**26**), 67.8 (**3**), 67.6 (**27**), 68.3 (**6**), 73.0 (**24**), 114.8 (**7**), 115.3 (**22**), 120.6 (**10**), 121.9 (**20**), 122.4 (**18**), 127.7 (**15**), 128.1 (**11**), 129.6 (**14**), 130.8 (**19**), 132.9 (**12**), 138.7 (**13**), 149.9 (**16**), 158.7 (**9**), 159.3 (**21**), 165.2 (**17**).

2 Additional dielectric measurements

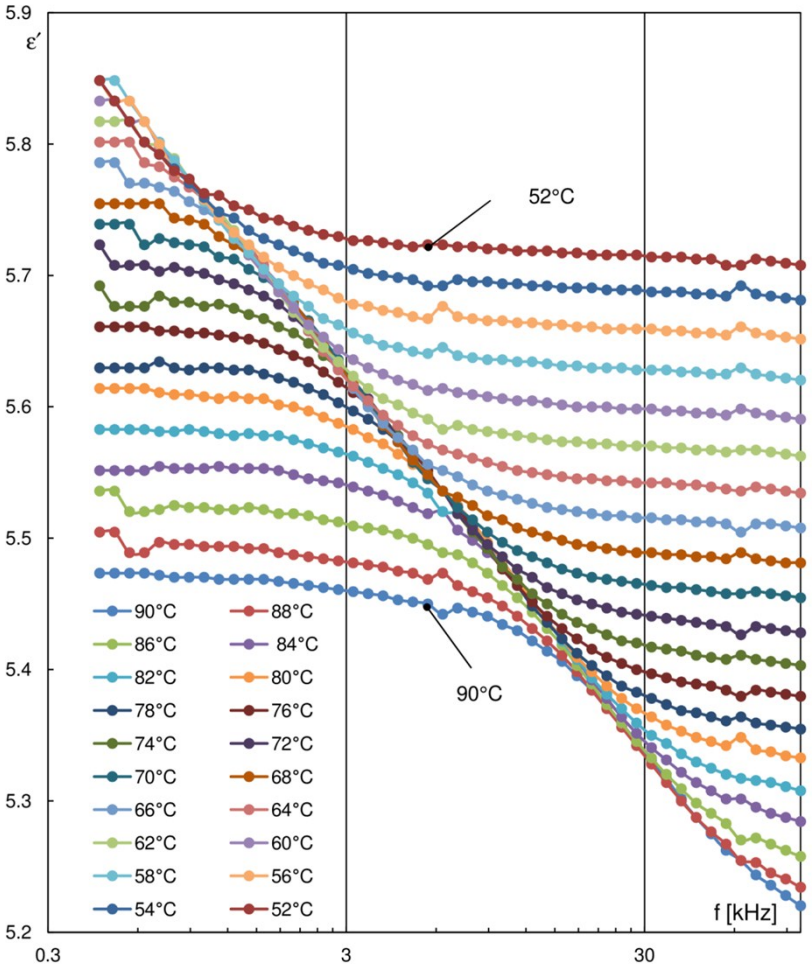

Figure A. Dielectric spectroscopy measurements for compound 3FOmC5 made in HG cell in temperature range for SmI phase: real part of electric permittivity ε′ versus frequency f. Frequency range is limited to the range where electric mode exists in SmI phase. One can see that for all curves it is easy to point the infection points. It means that relaxation frequency is easy to determine. Beside this, the inflection points move with the temperature (relaxation frequency increases at the temperature increase). Inflation point evolution with the temperature can suggest that mode fulfils the Arrhenius law. The dielectric increment δε read from the figure is rather low (~0.26).

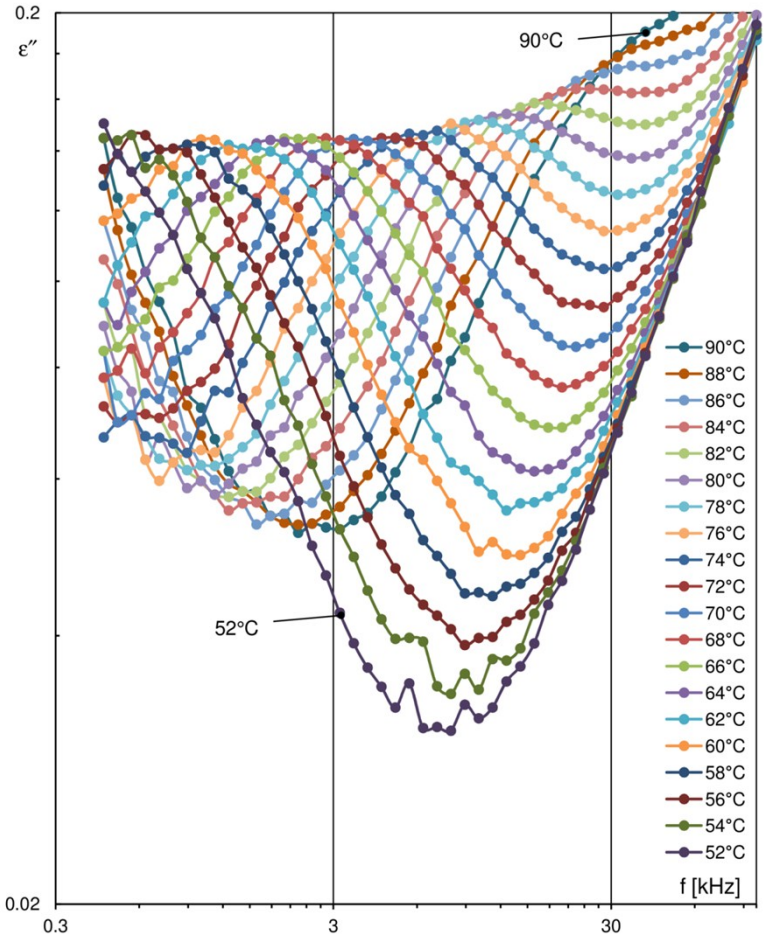

Figure B. Dielectric spectroscopy measurements for compound 3FOmC5 made in HG cell in temperature range for SmI phase: imaginary part of electric permittivity ε″ versus frequency f. Frequency range is limited to the range where electric mode exists in SmI phase. One can see that for all curves it is easy to point the maximum points. It means that relaxation frequency (corresponding to maximum point) is easy to be determined. For higher temperatures one cannot see the maximum point due to parasitic effect related to finite conductivity of ITO electrodes used in measuring cell. The dielectric increment δε read from this figure confirms the value read from the previous figure.

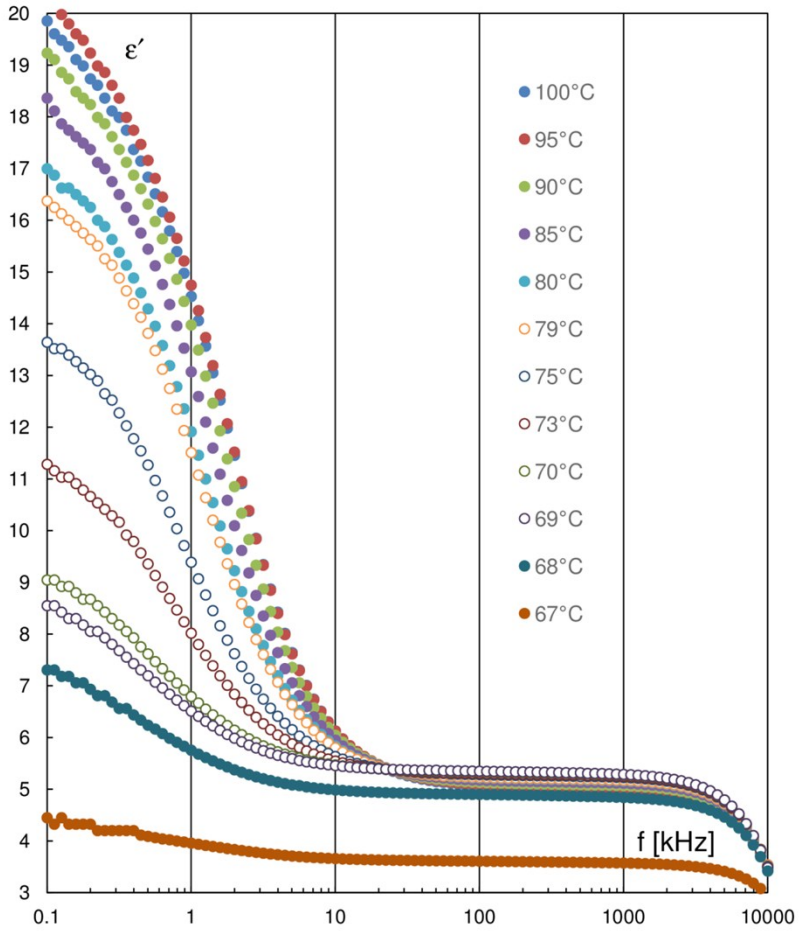

Figure C. Dielectric spectroscopy measurements for mixture 0.6 3FO3C1 + 0.4 3FO5C5, made in HG cell in temperature range for SmC* and SmI* phases: real part of electric permittivity ε′ versus frequency f. Frequency range is limited to the range of HP 4192A impedance analyzer. The shape of ε′(f) plots changes with temperature. One can see that for temperature range 100-80°C (full marks) dielectric strength δε of mode observed in SmC* slowly deceases with the temperature decrease. During further cooling, dielectric strength starts to decrease faster. Moreover the relaxation frequency, initially constant in SmC* phase, decreases at cooling in SmI* phase. The plots (open marks) suggest that SmI* phase temperature range is 10 degrees (79-69°C). Below 69°C (again full marks) the crystallization process starts and dispersion disappears. For all curves it is easy to point the infection points. It means that relaxation frequency is easy to determine. Beside this, the inflection points move with the temperature (relaxation frequency increases at temperature increase). The dielectric increment δε read for SmC* phase is around 13-15, while for SmI* phase it is between 11 (at 79°C) and 3 (at 69°C).

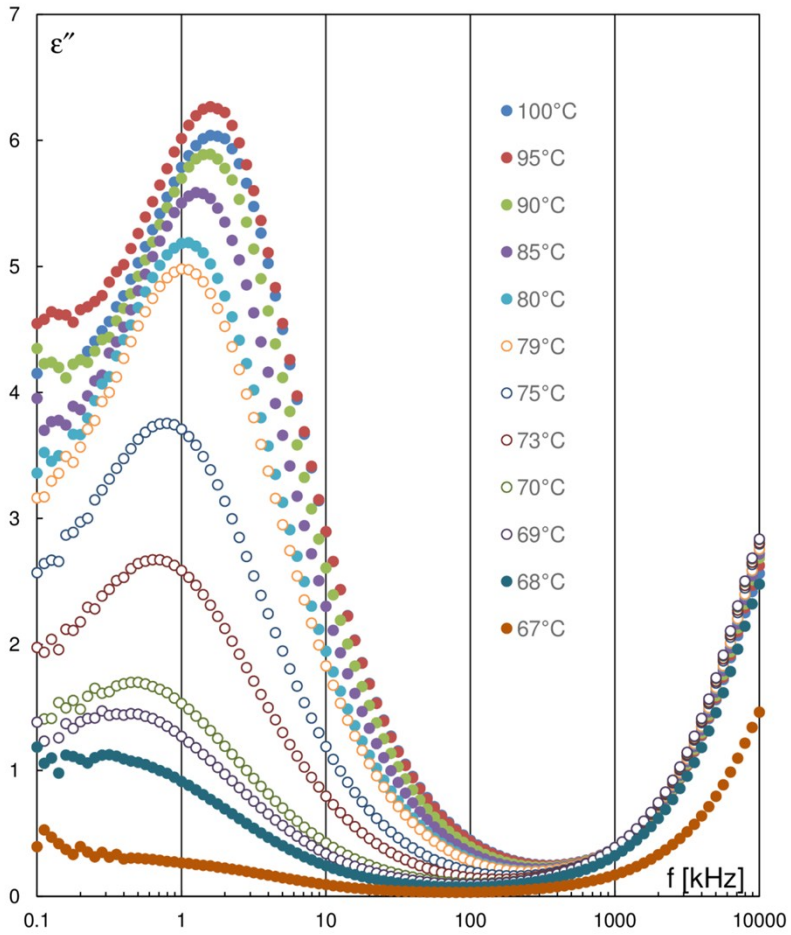

Figure D. Dielectric spectroscopy measurements for mixture 0.6 3FO3C1 + 0.4 3FO5C5, made in HG cell in temperature range for SmC* and SmI* phases: imaginary part of electric permittivity ε″ versus frequency f. Frequency range is limited to the range of HP 4192A impedance analyzer. One can see that for temperature range 100-80°C (full marks) dielectric strength δε of mode observed in SmC* slowly deceases with the temperature decrease. During further cooling dielectric strength starts to decrease faster. Moreover the relaxation frequency, initially constant in SmC* phase, decreases at cooling in SmI* phase. The plots (open marks) suggest that SmI* phase range is 10 degrees (79-69°C). Below 69°C (again full marks) the crystallization process starts and dispersion is smaller and smaller. For all curves it is easy to point the maximum points. It means that relaxation frequency is easy to be determined. Beside this, the maximum points move slowly with the temperature (relaxation frequency increases at temperature increase). The dielectric increment δε read from this figure confirms the values read from the previous figure.

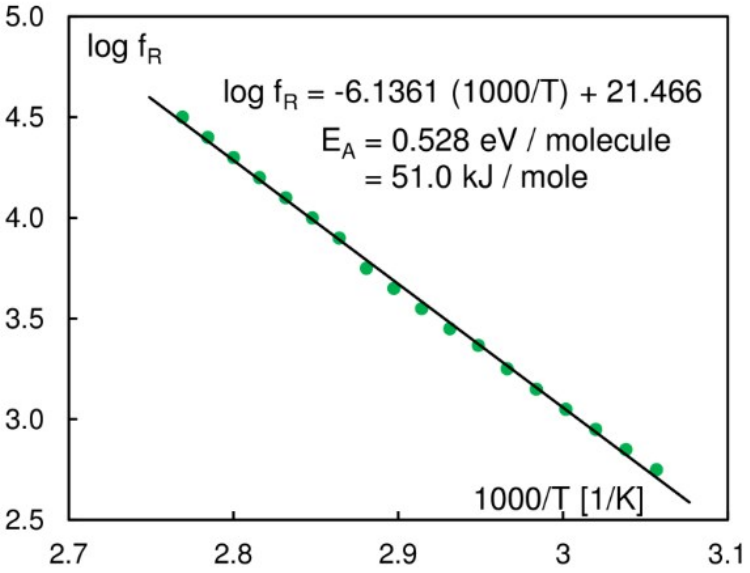

Figure E. The Arrhenius plot for the temperature range of 54-88°C, where the SmI phase exists in 3FO5C5 compound. An activation energy E_A calculated from the slope equals 0.528 eV/molecule (51.0 kJ/mole). The mode observed in the SmI phase is rather weak and exhibits rather constant dielectric strength δε, which changes from 0.27 at 68°C to 0.26 at 84°C.

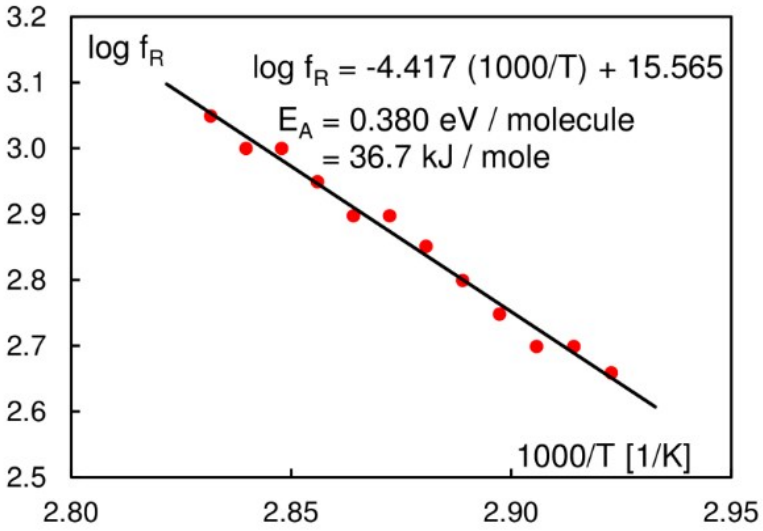

Figure F. The Arrhenius plot for the temperature range of 69-80°C, where the SmI* phase exists in the mixture: 0.6 3FO3C1 + 0.4 3FO5C5. The relaxation frequency changes continuously from the Goldstone mode in SmC* to the corresponding mode observed in the SmI* phase. The activation energy E_A (36.7 kJ/mole) of the mode observed in the SmI* phase, read from this plot, is comparable with the one shown for another mixture (35.2 kJ/mole)[I-II].

I M. Glogarova, D. Pociecha, E. Górecka, I. Rychetsky and J. Mieczkowski, *Ferroelectrics*, 2000, **245**, 43-50.

II A. Dwivedi, R. Dhar, V.K. Agrawal, R. Dąbrowski and D. Ziobro, *Mol. Cryst. Liq. Cryst*., 2011, **541**, 262-269